Article:
Liu, Q orcid.org/0000-0002-1132-9392, Qian, J, Barker, R orcid.org/0000-0002-5106-6929 et al. (3 more authors) (2021) Application of Double Loop Electrochemical Potentio-kinetic Reactivation for characterizing the intergranular corrosion susceptibility of stainless steels and Ni-based alloys in solar nitrate salts used in CSP systems. Engineering Failure Analysis, 129. 105717. ISSN 1350-6307

https://doi.org/10.1016/j.engfailanal.2021.105717

Application of Double Loop Electrochemical Potentio-kinetic Reactivation for characterizing the intergranular corrosion susceptibility of stainless steels and Ni-based alloys in solar nitrate salts used in CSP systems

Qingyang Liu[a,b], Jiong Qian[b,c], Richard Barker[a,b], Chun Wang[a,b], Anne Neville[a,b] and Frederick Pessu[a,b].

a. Institute of Functional Surface, School of Mechanical Engineering, University of Leeds, Leeds, LS2 9JT, United Kingdom.
b. Jiuli Corrosion and Integrity Centre Laboratory (University of Leeds), Leeds, LS2 9JT, United Kingdom.
c. Engineering Research Centre of High-Performance Nuclear Power Pipe Forming of Zhejiang Province, Huzhou 313028, China

Abstract

In this study, the sensitivity of four corrosion resistant candidate alloys; austenitic stainless steels (AISI 321 and AISI 347) and Ni-based alloys (IN 625 and In 825) to degrade by intergranular corrosion when used with molten salts in conditions of CSP systems were investigated at different temperatures. This was achieved by implementing the Double loop electrochemical potentiokinetic reactivation (DL-EPR) technique to quantitatively measure the degree of sensitisation (DOS) in the selected alloys by aging in air with and without Solar Salts (60 wt% $NaNO_3$ and 40 wt% KNO_3) at 550 - 750°C for 2 h. Electrochemical etching technique was implemented further to verify the results from DL-EPR. The results show that DL-EPR and microstructural evaluation techniques can be used to assess the synergy of temperature and molten salt electrochemical activities on the tendency for intergranular corrosion attack to occur in CPS systems. IN 625 showed the highest intergranular corrosion resistance among the alloys investigated in both air and molten salt; especially at temperatures higher than salt stability temperature. Samples aged in molten salts showed higher DOS than samples aged in air across all temperatures and linked to Cr-consuming corrosion and chemical reactions that drives molten salt – alloy interaction in CSP plants.

1. Introductions

With the rapid growth of world's population, increased industrialisation of emerging economies and the limitation of conventional energy sources, as well as the concern of potential impact of fossil fuel on global warming, there is strong motivation to explore alternative and renewable sources of energy [1]. In addition to other renewable resources (e.g. wind, geothermal and ocean), solar energy

is showing great promise. This is stimulated by the great amount of solar energy reaching the Earth [1, 2]. According to some estimates from International Energy Association, solar energy, if it is fully harnessed alone, can satisfy the world's total energy demand [3]. Electricity generation from solar irradiation is usually achieved by photovoltaic (PV) and photo-thermal [4] systems. However, concentrating solar power (CSP) has gained particular interest for large scale applications due to its advantage in terms of solar thermal energy production efficiency, low operation cost and low environmental impact. CSP systems are also integrated with thermal energy storage (TES) and heat transfer (HTF) systems [3] that rely on molten salts (solar salts) at temperatures ≥ 550°C. CSP systems are being deployed to mitigate the intermittence of supply of solar thermal electricity.

The electro-chemical aggressiveness of molten salts, high temperature conditions within CSP plants and the continuous interaction of molten salts with material surfaces increases the risk of corrosion, catastrophic failure of metallic components and reduce CSP plant efficiencies. Stainless steels and Ni-based alloys are widely used in CSP plants due to their good mechanical properties, high corrosion and oxidation resistance. Ni-based alloys are known to have superior resistance to pitting corrosion, crevice attack and stress corrosion cracking than stainless steels [1].

Intergranular corrosion is a form of localised corrosion which starts from the surface and develops inwards along the grain boundary to reduce cohesive stress, causing strength loss of material. It is linked with the segregation of impurities and/or depletion of one of the alloying elements along the grain boundaries (GBs). This is known as sensitisation and often used in reference to austenitic stainless steels and Ni-based alloys when operating in temperature range between 482-815°C [5]. Many researchers have concluded that the mechanisms and rate controlling step of classical intergranular corrosion is the chromium depletion and/or carbide precipitation [6]. Among reported theories in literatures, it was widely accepted that Cr carbides was the main cause of intergranular corrosion [7]. It is also believed that the process of precipitation of Cr carbide may be divided into reaction theory [8] and kinetic theory [9]. $M_{23}C_6$ carbide is the most prevailing carbide in stainless steels and its formation follows the reaction:

$$\mathbf{M_{23}C_6 \leftrightarrow 23M + 6C} \qquad \textbf{Equation 1}$$

The precipitation process of $M_{23}C_6$ includes the diffusion and reaction of Cr and C at the $M_{23}C_6$/matrix interface and the growth of $M_{23}C_6$ [10]. The diffusion coefficient of carbon is 10^4 larger than that of chromium due to the fact that carbon is present interstitially and chromium substitutionally [11]. S. Kolli [12] deduced that the preferential precipitation along the GBs is controlled by two factors, thermodynamics of the $M_{23}C_6$ formation and the difference in the diffusivities of Cr and C. After the formation of $M_{23}C_6$ at the grain boundaries, they become a kind of crystal defects with a higher Gibbs energy [10]. To reduce the Gibbs energy of the system, GBs tended to interact with other lattice defects (dislocations, vacancies and foreign atoms) [13] and thus lower the corrosion resistance of the material. Efforts and techniques have been taken to control or mitigate sensitisation of susceptible alloys, such as high temperature solution heat treatment, reducing carbon content to reduce carbide formation and incorporating strong carbide formers or stabilising elements such as niobium or titanium [6, 14-17]. Thorvaldsson and Dunlop [18-20] found that $M_{23}C_6$ was more stable than TiC and less than NbC, which is consistent with the finding formation of $M_{23}C_6$ in 321 after long term aging by Grot [21]. It is very important to determine the stabilised temperature to cause effective (Ti/Nb)C precipitation. Perrard [22, 23] found the kinetic

of NbC precipitation depend strongly on temperature and he built time–temperature transformation diagram to reveal the reaction rate between 600-800°C.

There has been limited research focused on characterising and understanding the relationship between molten salt chemistries, conditions encountered in CSP systems, the occurrence of sensitisation and the propensity for intergranular corrosion to occur in materials used in CSP systems. Chromium-depletion theory suggest that annealing at critical temperature or cooling slowly leads to the precipitation of carbides along the GBs [11], thus resulting in the local Cr content dropping below a critical level of 12 wt.% [15, 17]. In the region adjacent to GBs after precipitation, a minimum chromium content is unavailable to provide the passive Cr_2O_3 layer for corrosion resistance [12]. The working temperature range for molten salt is partly overlaid with the sensitisation temperature. This provides the basis for material degradation to be driven by the synergy of high temperature degradation and molten salt corrosion. The occurrence of sensitisation has been well researched for most alloys under high temperature conditions [15, 24]; particularly relating to alloy metallurgical and manufacturing processes [25]. Some authors have also reported intergranular corrosion attack in molten chloride [26, 27] and nitrate [28] salts. However, the propensity for sensitisation to occur in materials used with molten salt under real conditions in CSPs has not been researched and accurately characterised. Whilst the corrosion mechanism between chloride and nitrate salts has some similarities in terms of chromium removal from the alloy [29], the role of impurities in these salts introduces some distinct effect on material degradation; particularly for chloride molten salts [30]. Such research information is vital to guide material design and selection processes, improve CSP plant efficiency and lower energy production costs. Various standard tests have been developed to characterise the intergranular corrosion behaviour of stainless steels at different conditions. However, as a quick material selection filter, the double loop electrochemical potentiokinetic reactivation (DL-EPR) test can be used to quickly assess the synergy of electrochemical activity of molten salt and high temperature degradation of alloys used in CSP systems.

2. Experimental Methods

2.1 Materials

The materials used in this study were AISI 321 and AISI 347 austenitic stainless steels, and Inconel 625 and Incoloy 825 with nominal composition provided in Table 1. The as-received samples were heat treated by supplier at stabilised temperature for 5 h to cause effective (Ti/Nb) C precipitation [31]. These materials represent the main candidate materials used in CSP plants for molten salt transport and thermal collector pipes and accessories. The samples were cut from as – received pipes supplied by Zhejiang JIULI Hi-tech Metals Co., Ltd, China. Samples of approximately 1 cm^2 area were obtained from seamless pipes as shown in Figure S1. In this study, Solar salt (60 wt.% $NaNO_3$ and 40 wt.% KNO_3) was selected as experimental salt, which was purchased from Shanghai Chemical Reagents Limit Company with analytical reagent purity. The main impurities in this salt mixture includes 0.004% insoluble, 0.0001% IO_3^-, 0.004% Ca^{2+} and 0.001% NO_2^-. The salts were weighed according to the ratio and separately dried at 120 ˚C for 24 h in a furnace. Afterwards, they are heated at 300˚C for 24 h to a homogeneously mix of salt for further use.

2.2 DL-EPR test procedure

Prior to the DL-EPR test, the test samples were grounded with SiC paper up to 2000 grit, polished with 9 μm, 6 μm, 1 μm and 0.25 μm diamond suspension and then degreasing with acetone before experiments. The as-received materials were each solution heat treated at 1050°C for 0.5 h to dissolve all the potential NbC(N)/TiC(N), followed by water quenching (see Table 2) to get homogenised austenite field and destroy the sensitivity to intergranular corrosion due to the carbides entering into solution [11]. The treated samples were held and aged for 2 h at temperatures 550, 650 and 750°C in air without molten salt and in air with molten salt to simulate the temperature conditions in current and future CSP plants. . It should be worth noting that the temperature chosen in this study is based on the two key operational considerations. Firstly, athough the decomposition of nitrate salt [32] limits its use above 560 ˚C, the temperature at receiver panels (mainly made of Ni-based alloy) can reach to 650 ˚C when all the mirrors are engaged in reflecting solar irradiation at noon in the real solar power plants. A slightly higher limits are also possible with solar salt to realise a higher CSP plant efficiency targets [33]. Secondly, scientists are considering higher operation temperature (650 to 750 ˚C) of CSP plants in future [33] where hot tank, heat transfer pipes and receivers are made of Ni-based alloys in contact with other chloride and carbonate salts. The assessment of sensitization behaviours for Ni-based alloys or Stainless steels at higher temperature will provide theoretical basis and guidance for the characterisation and selection of the materials in the future.

DL-EPR tests were conducted in a three-electrode cell using a saturated calomel electrode (SCE) as reference electrode and platinum plate as counter electrode. The sample materials were embedded in epoxy resin and served as working electrode. The degree of sensitisation (DOS) of the aged samples were investigated in a solution of mixture of 2 M sulfuric acid (H_2SO_4) and 0.05 M potassium thiocyanate (KSCN) at 30 °C. The specimen was polarised anodically into passive region at 100 mV/min after exposure at open circuit potential (OCP) for 5 minutes. Once the passivation potential (typically 0.3V SCE) is reached, the scan was reversed from forward scan to reverse scan (cathodic direction) back to OCP at the same rate.

The peak current for the reverse scan and forward scan are recorded and named as reactivation current density (i_r) and activation current density (i_a) respectively. The ratio of reactivation (i_r) and activation (i_a) current density is defined as the degree of sensitisation. This is presented in Equation 2. After DL-EPR test, visual evidence to characterise materials susceptibility to IGC is obtained. The schematic DL-EPR curves is shown in Figure S2 obtained from the BS EN ISO 12732:2008 standard [34].

$$\mathbf{DOS = (i_r/i_a) \times 100\%} \qquad \textbf{Equation 2}$$

The correlation of anodic current and reactivation current with DOS is classified to three levels. DOS value less than 1% is an indication that material is ‘unsensitised’, 1%-5% means material is ‘slightly sensitised’ and higher than 5% indicates that material is ‘sensitised’ [34].

2.3 Metallographic etching procedure

The oxalic acid etch test was used for classification of etch structures in austenitic stainless steels according to ASTM A262 [35]. This etching procedure is usually used in conjunction with other evaluation test to provide a quick method to qualitatively assess material susceptibility to intergranular corrosion. 10% oxalic acid solution ($H_2C_2O_4.2H_2O$) was used to etch the surface of the salt/air exposed samples, and a section from the bulk metal, at 1 A/cm^2 for 1.5 min to evaluate any changes in microstructure to indicate material susceptibility to intergranular corrosion. The air-exposed and salt-exposed samples all went through another polish process prior to etching and examination, according to standard [35]. The microstructures obtained were classified into three types: “step” structure with no ditches at grain boundaries; “dual” structure, with some ditches at grain boundaries; and, “ditch” structure, with one or more grains completely surrounded by ditches [5]. According to ASTM A-262 [35], “ditch” structure, with one or more grains completely surrounded by ditches are more prone to IGC. These classification of microstructures after etching are adapted from ASTM A-262 and shown in Figure S3 [35].

2.4 Microstructure analysis

The microstructural observation and analysis of samples after the DL-EPR test were conducted using a Zeiss optical microscope (OM) (Axio Imager 2) and Carl Zeiss EVO MA15 scanning electron microscope (SEM). The SEM was integrated with an Oxford Instruments Aztec Energy dispersive X-ray (EDX) system with an 80mm X-max SDD detector which provided secondary and backscattered imaging, EDX elemental mapping and line scans. The working voltage of SEM is set at 20 kV and working distance of 12–13 mm.

3. Result and discussion

3.1 The microstructure

Figure 1, Figure 2, Figure 3 and Figure 4 show the SEM micrographs for as-received samples of AISI 321, AISI 347, IN 625 and In 825. EDX/EDS mapping images are also presented in each figure. Titanium stabilised AISI 321 and Niobium stabilised AISI 347 austenitic stainless steels have an austenite phase with equiaxed-grain size about 40-50 μm prior to sensitisation treatment. Referring to the backscatter image, there are some precipitates distributed along the GBs or inner grain. SEM/EDX element mapping shows that the (Fe, Ni and Cr) depleted precipitate are identified as TiN and TiC in AISI 321 and NbN in AISI 347, which is consistent with the reports by A.Pardo [14]. IN 625 and In 825 show the austenitic phase with equiaxial grains and some annealing twins formed during the heat treatment process. There is also some precipitation along the GBs or inner grain, which was identified as NbN or TiN in Figure 3 and Figure 4.

3.2 DOS results

The DL-EPR curves of sensitised samples of AISI 321 AISI 347 IN 625 and In 825 were shown in Figure 5, Figure 6, Figure 7 and Figure 8, respectively. The critical current and DOS values determined from the DL-EPR curves are summarised in Table S1 and plotted in Figure 9 and Figure 10 as function of temperature and effect of molten salt on degree of sensitisation. Referring to Figure 1, Figure 2, Figure 3 and Figure 4 and grade regulation for characterising DOS in BS EN ISO 12732:2008 standard [34], the solution treated as-received samples are unsensitised.

3.2.1 AISI 321

According to the DL-EPR curve shown in Figure 5, air-sensitised AISI 321 samples shows a relatively small reactivation current density at the temperatures under focus. Referring to Table S1 and Figure 9, DOS value increase gradually from 0.1% to 0.18% with increase of temperature from 550˚C to 750˚C. In air, the AISI 321 clearly exhibited no tendency for intergranular corrosion to occur after 2 h heat treatment at 750˚C with a DOS value of 0.18%. These results are consistent with the results of microstructure observation. In Figure 11 (a, b, c), the samples exhibited 'step' structure without any Cr-depletion or Cr precipitation evidence at GBs. Ti-stabilised AISI 321 steels are less prone to IGC and exhibited no obvious change in microstructure with increase in aging temperature in air. However, the specimens exhibited higher tendency for IGC to occur in solar salt than in air from the result of DL-EPR at same temperature in Figure 9. The DOS value of samples in solar salt increases to 0.23% and 0.34% at 550˚C and 650˚C, respectively. However, these samples remained 'unsensitised' as the DOS values are less than 1%. The results of microstructure also confirm this conclusion as samples exhibited 'step' structure when aged at 550˚C and 650˚C in molten salt, as shown in Figure 11 (d) and (e). It is worth mentioning that there is significant increase in DOS value from 0.18% in air to 4.27% in solar salt at 750˚C. At 750˚C and in solar salt, the microstructure of AISI 321 samples exhibited 'dual' structure with some ditches at GBs as shown in Figure 11 (f), indicating the highest tendency for IGC to occur.

In this study, the DOS of AISI 321 increases with increasing temperature while the synergy of high temperature and the aggressive nature of solar salt significantly increases the tendency for AISI 321 to degrade by IGC. As reported in the literature [36], chromium carbides precipitate most when aging at temperature between 750-800 ˚C without any effective TiC precipitation in AISI 321 samples [31]. On one hand, the increase of temperature can enhance the formation of chromium carbide thermodynamically and kinetically, resulting in significant increase of DOS value. On the other hand, the chemical reaction with molten salt is also a Cr-consuming process that leads to the formation of corrosion products such as iron chromium spinel and chromium nickel oxide [(Fe, Ni) Cr_2O_4] [1, 37, 38]. Therefore, the degree of sensitisation, and hence the likelihood for AISI 321 to degrade, could be enhanced by the synergy of increase of temperature and molten salt chemistry.

3.2.2 AISI 347

Figure 6 shows the DL-EPR curves of AISI 347 sensitised at 550, 650 and 750 for 2 h in air and molten salt. The DOS value of air sensitised AISI 347 samples is 0.29%, 0.34% and 0.24% when held at 550˚C, 650˚C and 750˚C. Although this was slightly higher than the DOS of AISI 321 samples, AISI 347 also show lower tendency for IGC to occur with DOS less than 1% and therefore considered as 'unsensitised', even at 750°C. These conclusions are consistent with the results from microstructure observation. Air sensitised AISI 347 specimen shows 'step' structure in Figure 12 (a), (b) and (c) for test at 550˚C, 650˚C and 750˚C, respectively.

In the molten salt system, AISI 347 samples show the 'step' structure at 550˚C and 750˚C and 'dual' structure when aged at 650˚C in Figure 12 (d), (e) and (f). As mentioned before, specimens tend to have a higher tendency for IGC to occur when they have ditch structure than dual structure and step structures. The DOS value of samples in solar salts were 0.36%, 1.09% and 0.45%, which is slightly higher than when samples were aged in air at corresponding temperature. The sample aged at 650˚C in molten salt also shows a 'dual' structure (shown in Figure 12 (e)) with highest DOS value, indicating highest tendency of IGC to occur. This indicates that samples aged at 650 ˚C in both air and molten salt showed higher DOS values and hence higher tendency for IGC to occur than samples aged at 550˚C and 750˚C in both air and molten salt. This threshold effect with respect to DOS is linked to the preferred temperature limit for NbC precipitation suggested by Perrard [22, 23] and Stopher [39]. Both authors [22, 39] came to the conclusion that NbC precipitation depends strongly on temperature and precipitation occurred fastest between 700-800°C (973K-1073K). More stable NbC [40] precipitation could retard the precipitation of Cr carbides and thus reduce the IGC tendency. From this study, it is clear that there is a "critical sensitisation" temperature of 650˚C in molten salts at which AISI 347 samples exhibited highest DOS and tendency for IGC to occur. This is consistent with the findings of Perrard [23] and Stopher [39]. The trend of increase in DOS values in molten salt in AISI 347 is similar to AISI 321 to highlight the contribution of molten salt chemistries to the Cr-consuming interfacial phenomenon that increases the tendency for IGC to occur.

3.2.3 IN 625

In addition to testing austenitic stainless steels, electrochemical test and etching method was also used to investigate Ni-based alloy. These tests have been shown to be suitable for characterising the DOS in Ni-based alloys [41, 42]. Referring to Figure 7 and Figure 8 for IN 625 and In 825 respectively, the DL-EPR curves and results of Ni-based alloys were significantly different from austenitic stainless steels in terms of current density and reactivation process. The results indicate that alloy composition has a strong effect on anodic and reactivation process even though sensitisation may lead to similar chromium depletion.

IN 625 exhibited the lowest tendency for IGC to occur in air at 550-750°C without any reactivation peaks (shown in Figure 7 (a)). The samples remained passive during anodic and reactivation scan.

The microstructure of IN 625 samples after aging in air shows a shallow 'step' structure in Figure 13 (a), (b) and (c) to confirm the results obtained from DL-EPR test. The DL-EPR curves of IN 625 samples aged in solar salt is shown in Figure 7 (b). Two reactivation peaks to obtain increase in DOS values of 30.4% and 23.1% at 650°C and 750°C respectively between air and molten salt can be observed. 'Step' structure for IN 625 at 550°C and 'ditch' structure at 650°C and 750°C is a clear indication that IN 625 samples remained unsensitised at 550°C even with molten salt but severely sensitised at 650°C and 750°C. This result shows that temperature plays a decisive role on sensitisation behaviour of IN 625 in molten salt. More detailed analysis is provided in section 3.3.

3.2.4 In 825

Similar to IN 625, In 825 samples exhibited relatively small anodic and reactivation current in the DL-EPR curves. In comparison with IN 625, DL-EPR tests on In 825 samples in air show the anodic peaks and reactivation peaks at all temperature in Figure 8 (a). The DOS values were 10.0%, 31.6% and 35.2% at 550, 650 and 750°C respectively, indicating that In 825 samples are "sensitized" in air. 'DL-EPR results and Ditch' structure in Figure 14 (a), (b) and (c) for In 825 aged in air show relatively higher tendency for IGC to occur. For DL-EPR tests with molten salt, the DOS value of In 825 samples was 49.4%, 76% and 65.5% at 550, 650 and 750°C, respectively in Figure 8 (b). These values are significantly higher than the DL-EPR test results on IN 825 samples aged in air at all temperatures. Similarly, In 825 samples aged in solar salts exhibited 'ditch' structure after electrochemical etching as shown in Figure 14 (d), (e) and (f). The width of Cr-depleted zones are the largest and indicate the highest tendency for IGC to occur [8] among all the alloys investigated. In 825 samples exhibit high sensitivity to temperature when aged in air and in molten salt. From these results, it is believed that In 825, though a Ni-based alloy, exhibited a significantly higher tendency for IGC to occur than Ti and Nb – alloyed austenitic stainless steels.

3.3 Sensitisation mechanism with and without molten salt

As earlier discussed, the sensitisation behaviour of stainless steels and Ni-based alloys are often due to the precipitation of chromium carbides at grain boundaries. This therefore leads to a chromium depleted area at/near the GBs, where a minimum chromium content is unavailable to provide the passive film or passive films break during the reactivation process. Both scenarios could cause the depleted area to be vulnerable to intergranular corrosion, exhibiting the rise of reactivation current and high DOS value. For austenitic stainless steels, the most accepted explanation for sensitisation is the Cr-depletion theory. Other researchers [43] have suggested that the size and Cr content of the Cr-depleted zone are the main factors driving intergranular corrosion. Yin [8] later reported that the degree of sensitisation of stainless steels is only determined by the width of Cr-depleted zone. The formation of Cr-depleted area is due to the lower diffusion coefficient of chromium than that of carbon.

In this study, the width of Cr-depleted area was not investigated, however, the results from post experiment analysis shows evidence of the tendency for IGC to occur along the grain boundaries. This has been observed in this study to increase with increasing of temperature and in synergy with

molten salt for AISI 321 (see Figure 11). The effect of temperature on sensitisation behaviour for stainless steels is linked to the degree of carbide precipitation ($Cr_{23}C_6$, TiC or NbC in Figure 1-Figure 5) at critical temperature. The higher degree of sensitisation in molten salt was due to the corrosion and chemical reaction kinetics that consumes Cr content. Solar salt is known to remain stable at temperatures ≤ 565°C and decomposes at higher temperatures into nitrite and oxygen ions [29], which enhanced the corrosivity of salt. This process in synergy with the high temperatures triggers aggressive reaction with bulk material to form corrosion products, such as mixed oxides of (Cr, Fe and Ni) [44]. Chromium rich corrosion products could result in Cr-depleted zones, where passive film breakdown occurs and are likely to corrode actively. For Ni-based alloys, the reason why molten salt causes the increased degree of sensitisation is similar with that of stainless steels.

The sensitization mechanism is presented as a schematic illustration in Figure 15 to summarise the mechanism of sensitisation behaviour and synergy of temperature and molten salt to influence the tendency for IGC to occur. When "sensitised" samples precipitate Cr-carbide along GBs, inner chromium is hindered more significantly in its ability to diffuse outwards than carbon, thus leading to a Cr-depleted area. More Cr carbides aggregate at the grain boundaries due to the higher diffusion coefficient of Cr with the increase of temperature, thus increasing the width of Cr-depleted area and the tendency for IGC. While in molten salt, according to literature [1, 29, 45], oxidation was the primary attack to the alloys and the formation of Cr and Fe oxides may protect the bulk material against the corrosion. However, the subsequent dissolution of the Cr oxides into molten salt [29, 46] causes the breakdown of this protective film and facilitates the interaction between molten salt and bare metal/alloy to accelerate the consumption of Cr emanating from bulk material as temperature increase. This corrosion/oxidation and dissolution process will remove chromium from the GBs first. Then, due to faster diffusion through GBs at temperatures below about 800 °C, it will lead to higher sensitisation near the exposed surface. Therefore, in the presence of molten salt, more chromium was consumed and Cr-oxides dissolved from the inner grain and along GBs, increasing the width of Cr-depleted area and the tendency for IGC to occur. The dissolution of Cr-oxide into molten salt resulted in higher DOS in molten salt than that in air by consuming chromium adjacent to GBs.

It is worth mentioned that the anodic and reactivation current of Ni-based alloy is almost four orders of magnitude lower than that of stainless steels, indicating that the passive film is more stable than that on stainless steels. We can conclude that the passive film on the surface of Ni-based alloys are containing mixture oxides of chromium and nickel due to its higher nickel content, which exhibited a more stable oxide layer at higher temperature; particularly for IN 625, than the chromium oxide film on the surface of stainless steels. Further long-term immersion tests in molten salt are needed to investigate the IGC behaviour to confirm this particular conclusion.

4. Conclusion

As a non-destructive and time saving test method, Double loop electrochemical potentiokinetic reactivation test has been successfully deployed to quantitatively evaluate the degree of sensitisation and characterise material susceptibility to intergranular corrosion.

The following conclusions have been deduced from this research:

1. The tendency for intergranular corrosion to occur in molten salt was shown to be influenced by the synergy of temperature and molten salt chemistry for different alloys; AISI 321, AISI 347, IN 625 and IN 825. Degree of sensitisation was higher for samples aged in molten salt than for samples aged in air and linked to the relationship between the kinetics of metal carbide precipitation and aging temperature in synergy with molten salt corrosion and chemical activities.

2. The higher DOS value of samples aged in salts than samples aged in air is linked to can be linked to the underpinning Cr-consuming reactions that drives electrochemical and chemical interactions metals and molten salt. Therefore, more chromium was consumed both in the inner grains and along GBs, increasing width of Cr-depleted area and promoting the likelihood for intergranular corrosion to occur.

3. A temperature threshold effect was also observed for AISI 347 above which DOS and hence the tendency for IGC to occur reduces. This was also observed in the microstructure change for AISI 347 from a dual structure at 650°C to a step structure at 750°C in molten salt and linked to the threshold effect of temperature on the kinetics of NbC precipitation. Increase in the kinetics of NbC precipitation at 750°C decreases the kinetics of Cr-C precipitation and hence decreased tendency for IGC to occur.

4. IN 625 has highest IGC resistance among these steels from the results of microstructure observation and DL-EPR with or without molten salt in this study. Stainless steels exhibited higher intergranular corrosion tendency when employed at sensitised temperature with molten salt.

Data availability

The raw/processed data required to reproduce these findings cannot be shared at this time as the data also forms part of an ongoing study.

CRediT authorship contribution statement

Qingyang Liu: Conceptualization, Methodology, Formal analysis, Investigation, Resources, Writing - original draft. **Jiong Qian**: Review & editing. **Richard Barker**: Supervision, Writing - review & editing. **Chun Wang**: Supervision, Writing - review & editing. **Anne Neville**: Resources, Review & editing, Supervision. **Frederick Pessu**: Supervision, Methodology, Writing - review & editing, Resources, Conceptualization.

Declaration of Competing Interest

The authors declare that there is no conflict of interest.

Acknowledgement

The authors acknowledge the funding and support from Zhejiang JIULI Hi-tech Metals Co., Ltd through the Jiuli Hi-tech Metals Co – University of Leeds corrosion integrated centre.

5. Tables and figures

Table 1 Chemical compositions of austenitic stainless steels and Ni-based alloys

Material	C	Mn	Ni	Si	P	S	N	Al	Cr	Fe	Mo	Ti	Nb	PREN
AISI 321	0.018	1.44	9.24	0.519	0.0347	0.0011	0.014	-	17.33	Bal.	-	0.225	-	17.55
AISI 347	0.049	0.95	9.65	0.402	0.026	0.0043	0.086	0.0027	17.35	Bal.	-	-	0.656	18.7
IN 625	0.018	0.039	62.36	0.142	0.00059	0.0025	0.0075	0.261	21.69	3.06	8.65	0.211	3.31	50.36
In 825	0.008	0.673	40.18	0.258	0.0119	0.0009	0.0092	0.104	22.6	30.32	2.88	0.943	0.025	32.25

Notes: a. Titanium stabilized AISI 321 and niobium stabilized AISI 347

b. PREN=Cr+3.3×(Mo+0.5×W) +16×N

Table 2 Time-temperature profile for sensitizaition test

Materials	**Heat treatment**	**Temperature (°C)**	**Holding time(h) without salt**	**Holding time(h) in molten salt**
AISI 321	Solution and water quenching	1050	0.5	0
AISI 347	As received			
In 825	DL-EPR experiment	550	2	**2**
IN625		650	2	**2**
		750	2	**2**

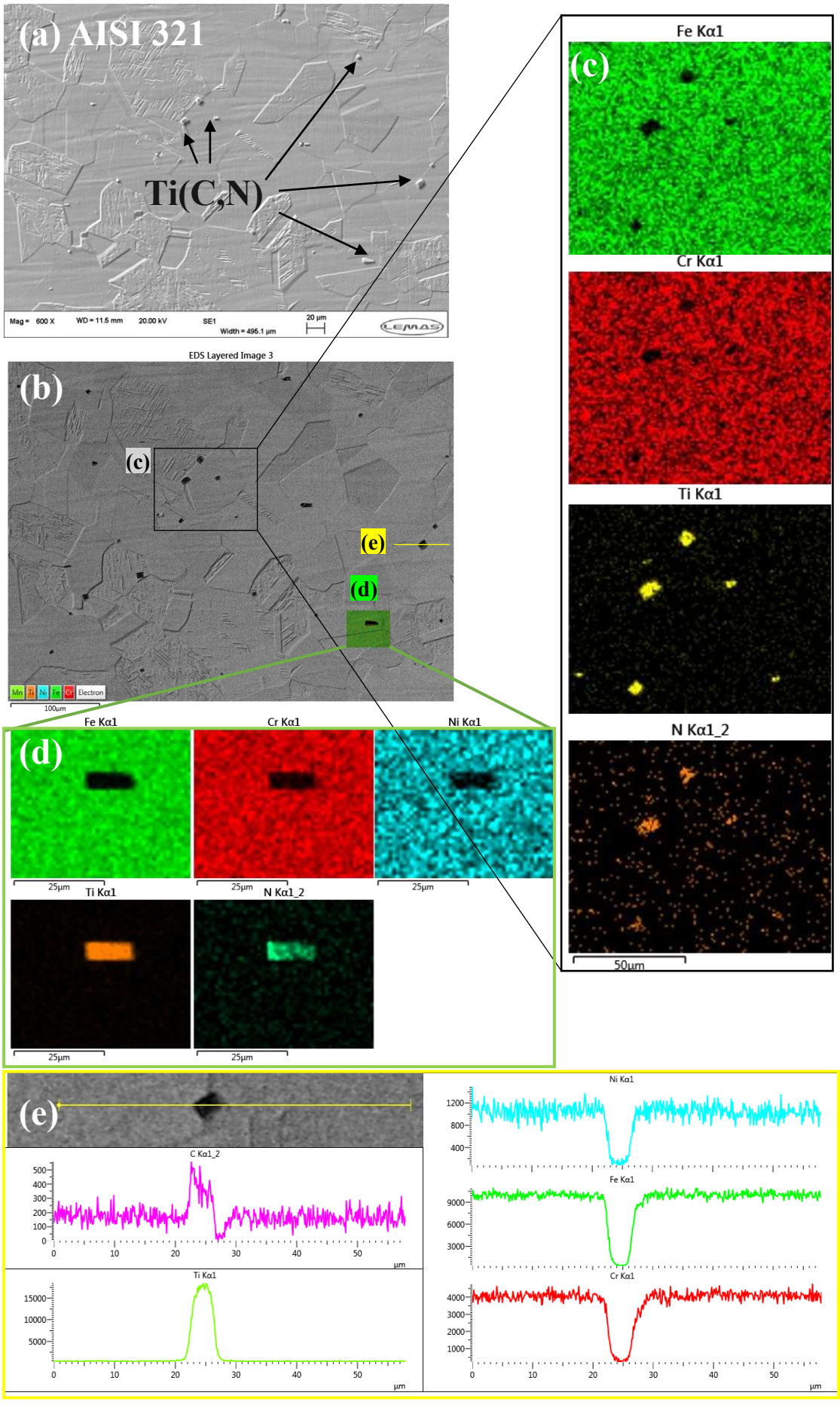
(a) AISI 321
Ti(C,N)
Mag = 600 X
WD = 11.5 mm
20.00 kV
SE1
Width = 496.1 µm
20 µm
EDS Layered Image 3
(b)
(c)
(d)
(e)
Electron
100µm
Fe Kα1
Cr Kα1
Ti Kα1
N Kα1_2
50µm
Ni Kα1
25µm
(d)
(e)
C Kα1_2
Ti Kα1
Ni Kα1
Fe Kα1
Cr Kα1
µm

Figure 1 The microstructure of as-received AISI 321 (a) SEM image; (b)BSE image;(c) EDS element mapping of black box in (b); (d) EDS element mapping of green box in (b); (e) EDS line scan of yellow line in (b).

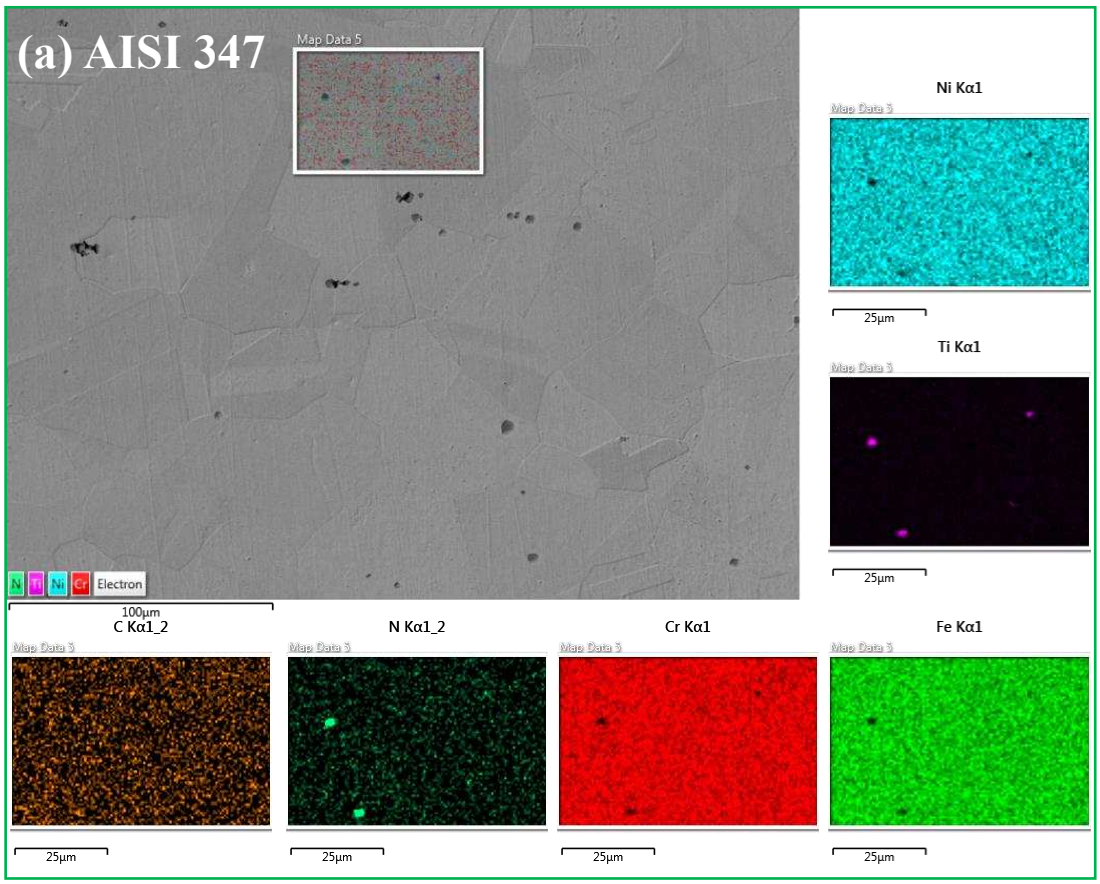

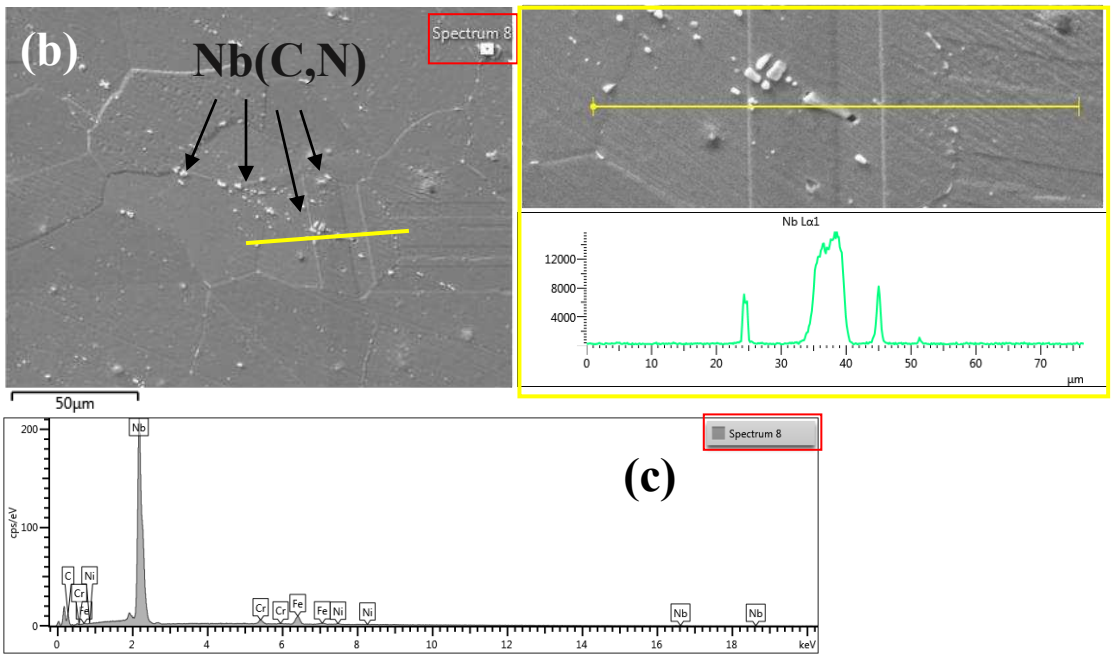

Figure 2 The microstructure of as-received AISI 347 (a) BSE image with element mapping; (b)SEM image with element line scan; (c) EDS point profile in (a)

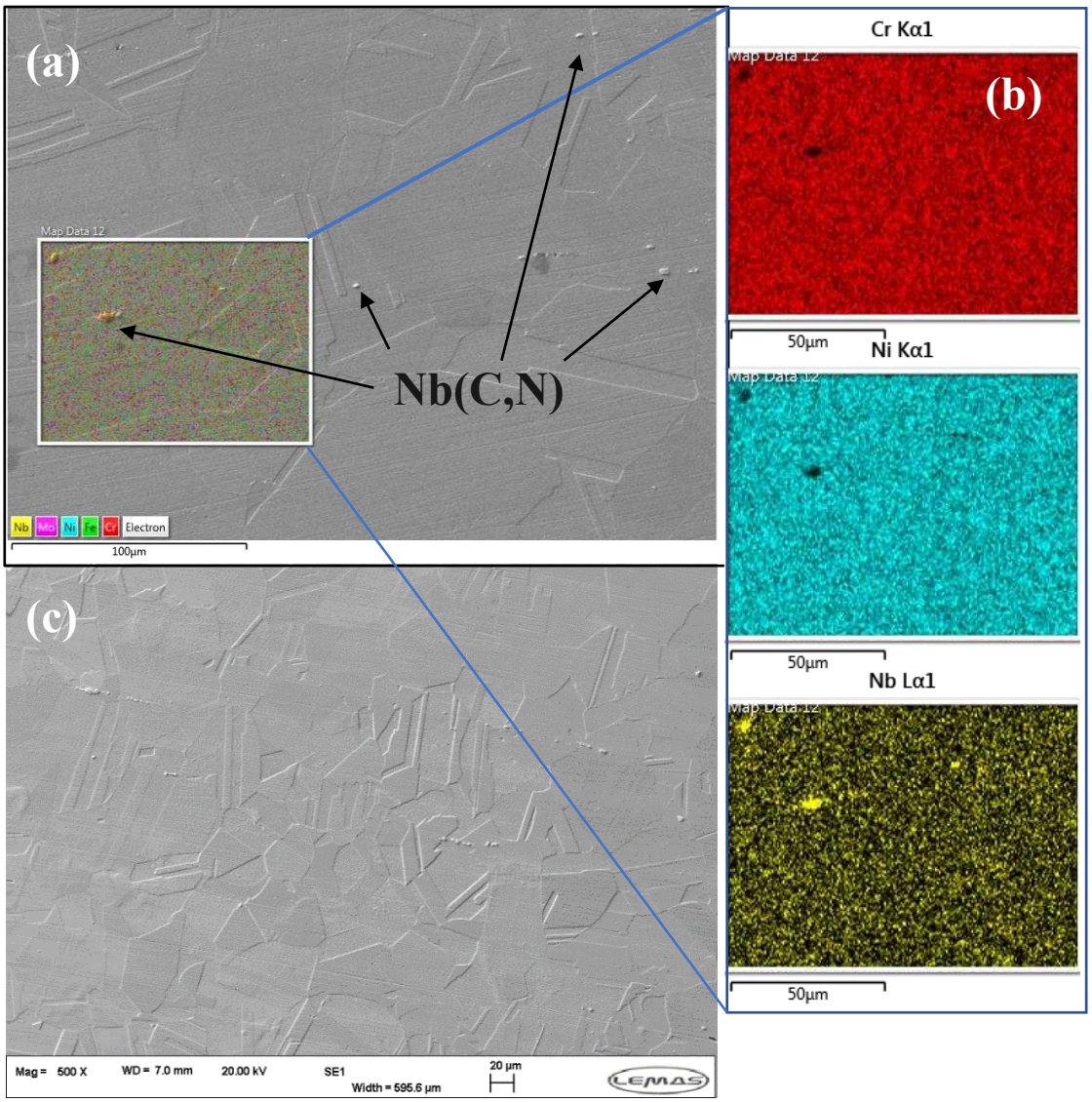

Figure 3 The microstructure of as received IN 625 (a) and (c) SE image (b) EDS mapping profile of white box in (a). Ti EDS mapping is unavailable due to lower content compared with Nb in IN 625.

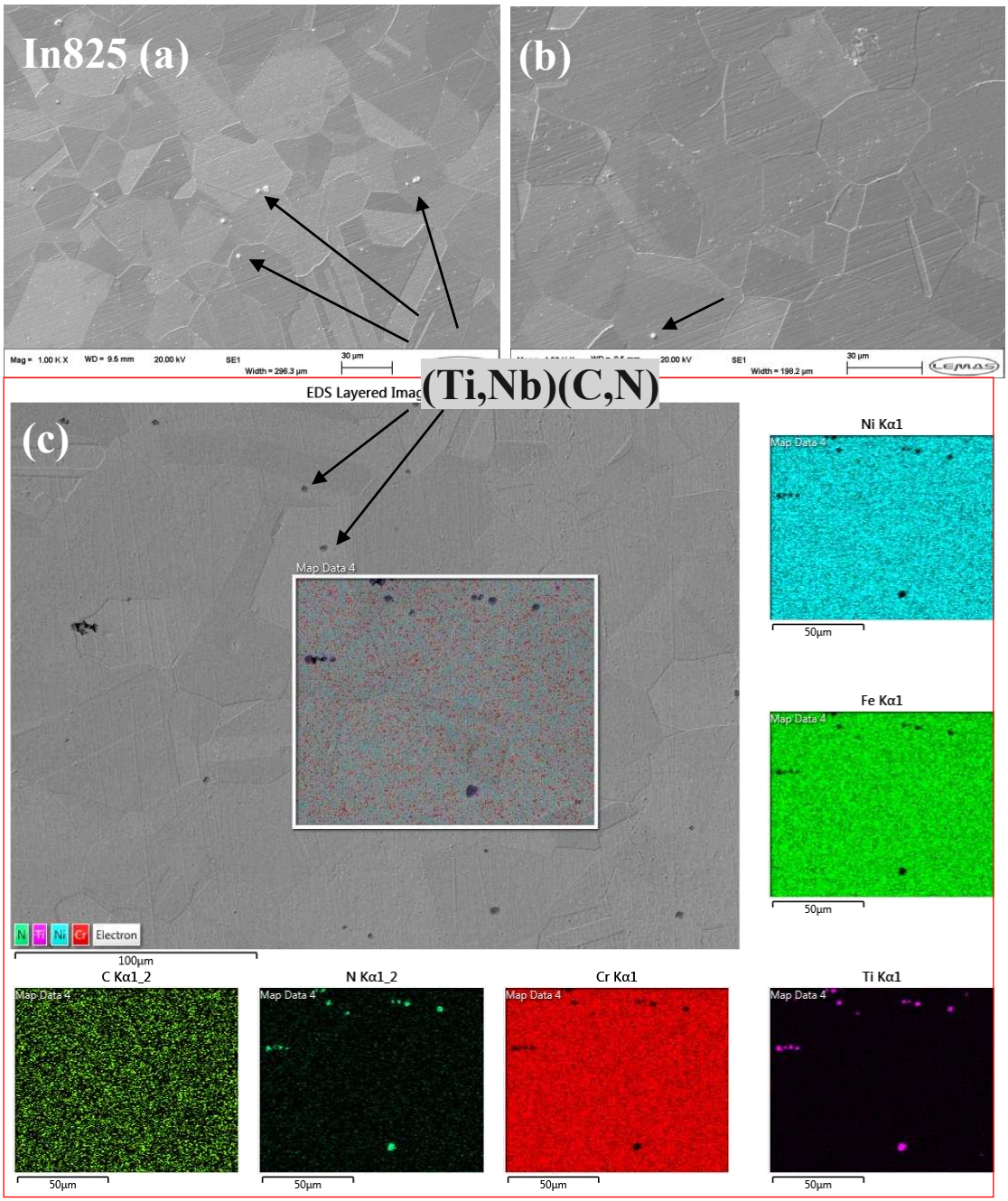

Figure 4 The microstructure of as received In 825 (a) and (b) SE images under different magnification; (c) EDS mapping profile. Nb EDS mapping is unavailable due to lower content compared with Ti in In 825.

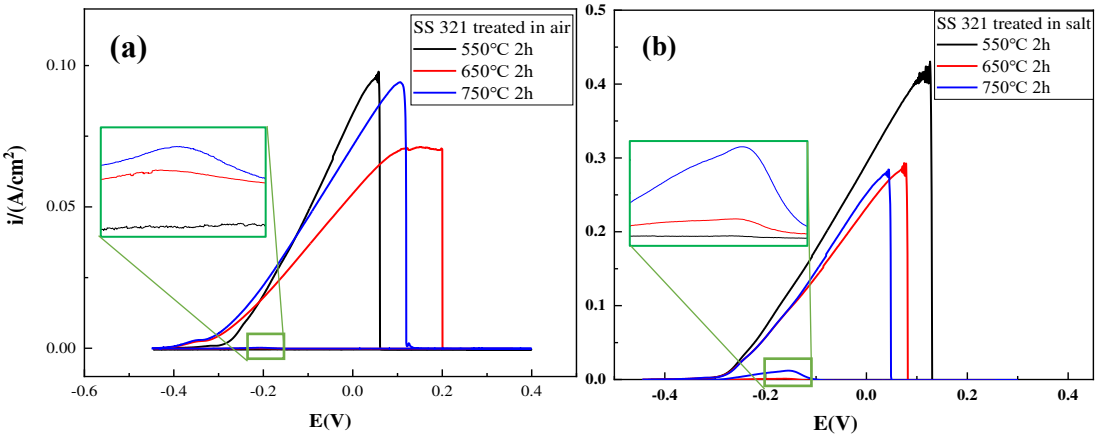

Figure 5 DL-EPR curves of AISI 321 sensitised at 550, 650 and 750 for 2 h in air and molten salt

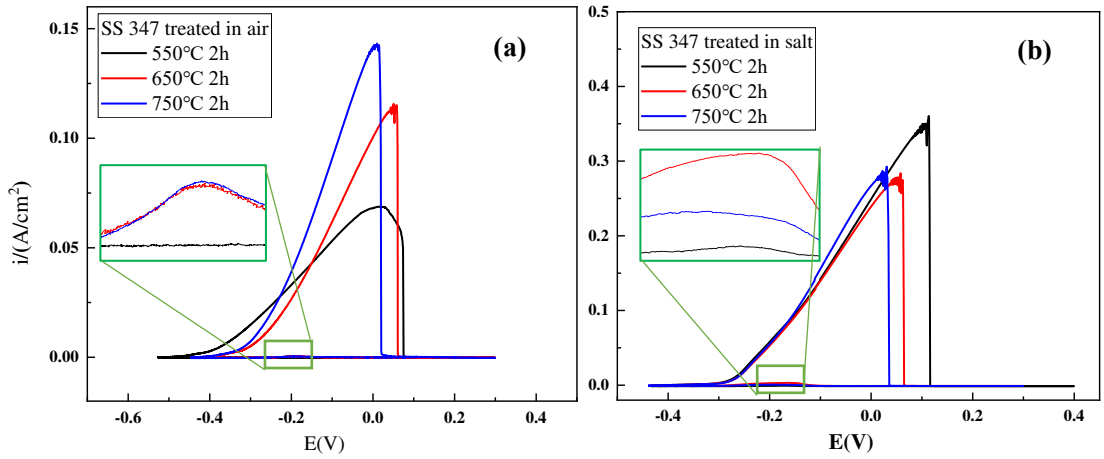

Figure 6 DL-EPR curves of AISI 347 sensitised at 550, 650 and 750 for 2 h in air and molten salt

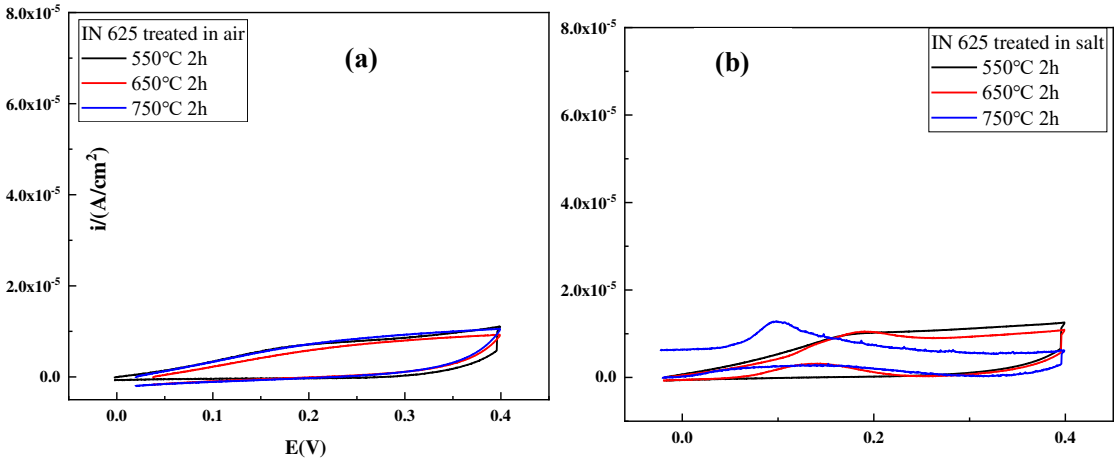

Figure 7 DL-EPR curves of IN 625 sensitised at 550, 650 and 750 for 2 h in air and molten salt

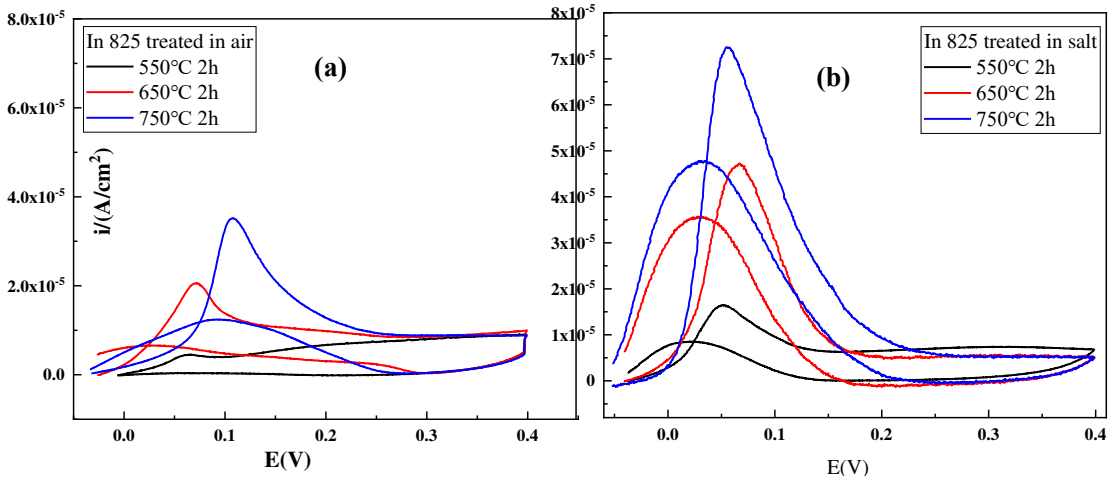

Figure 8 DL-EPR curves of In 825 sensitised at 550°C, 650°C and 750°C for 2 h in air and molten salt

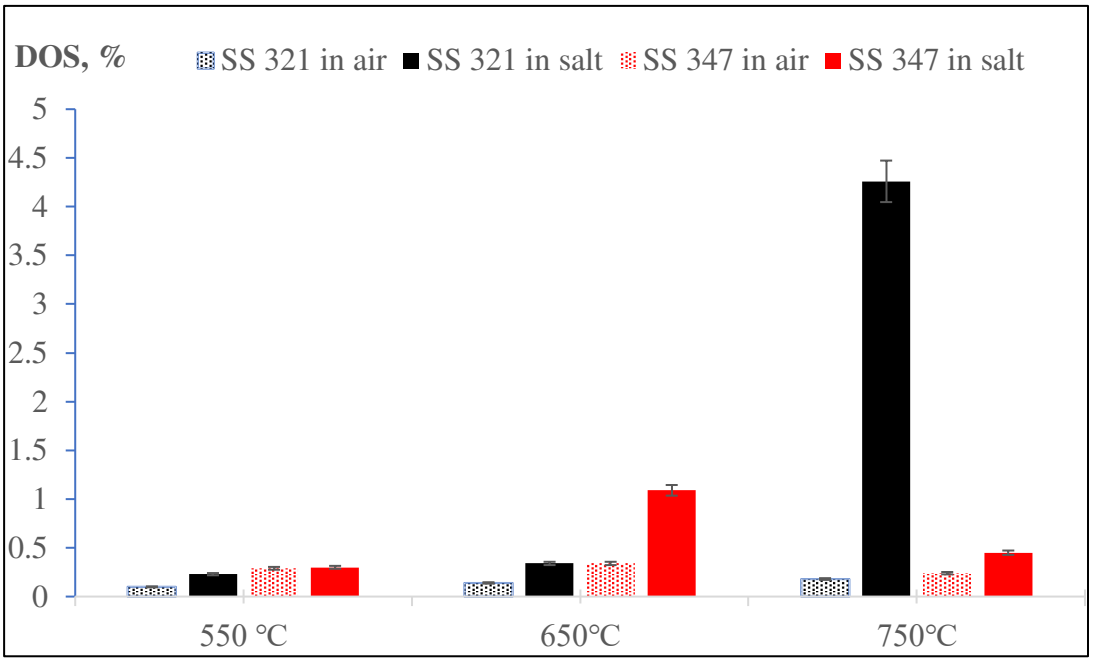

Figure 9 Bar chart of DOS value as function of temperature and molten salt for AISI 321 and AISI 347

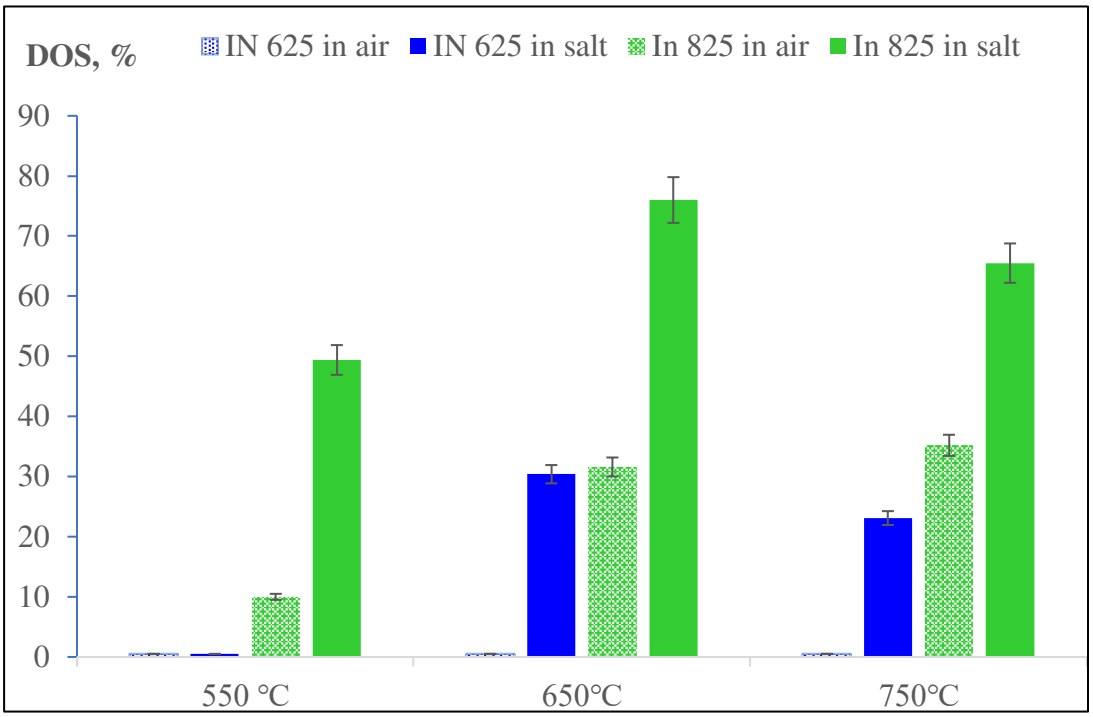

Figure 10 Bar chart of DOS value as function of temperature and molten salt for IN 625 and In 825

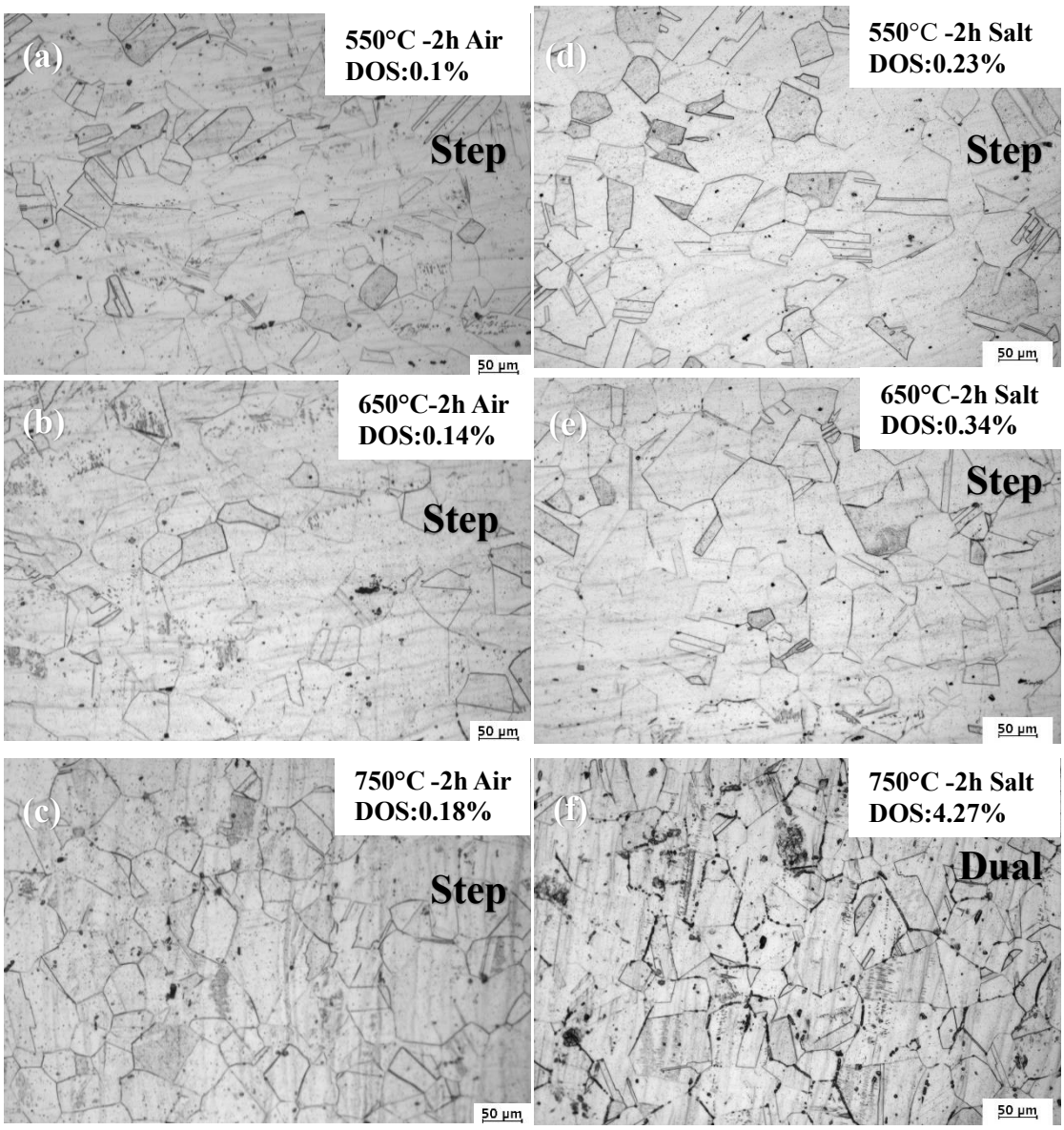

Figure 11 Oxalic etching microstructures for AISI 321 treated by (a) 550°C for 2 h in air; (b) 650°C for 2 h in air; (c) 750°C for 2 h in air; (d) 550°C for 2 h in molten salt; (e) 650°C for 2 h in molten salt; (f) 750°C for 2 h in molten salt, respectively.

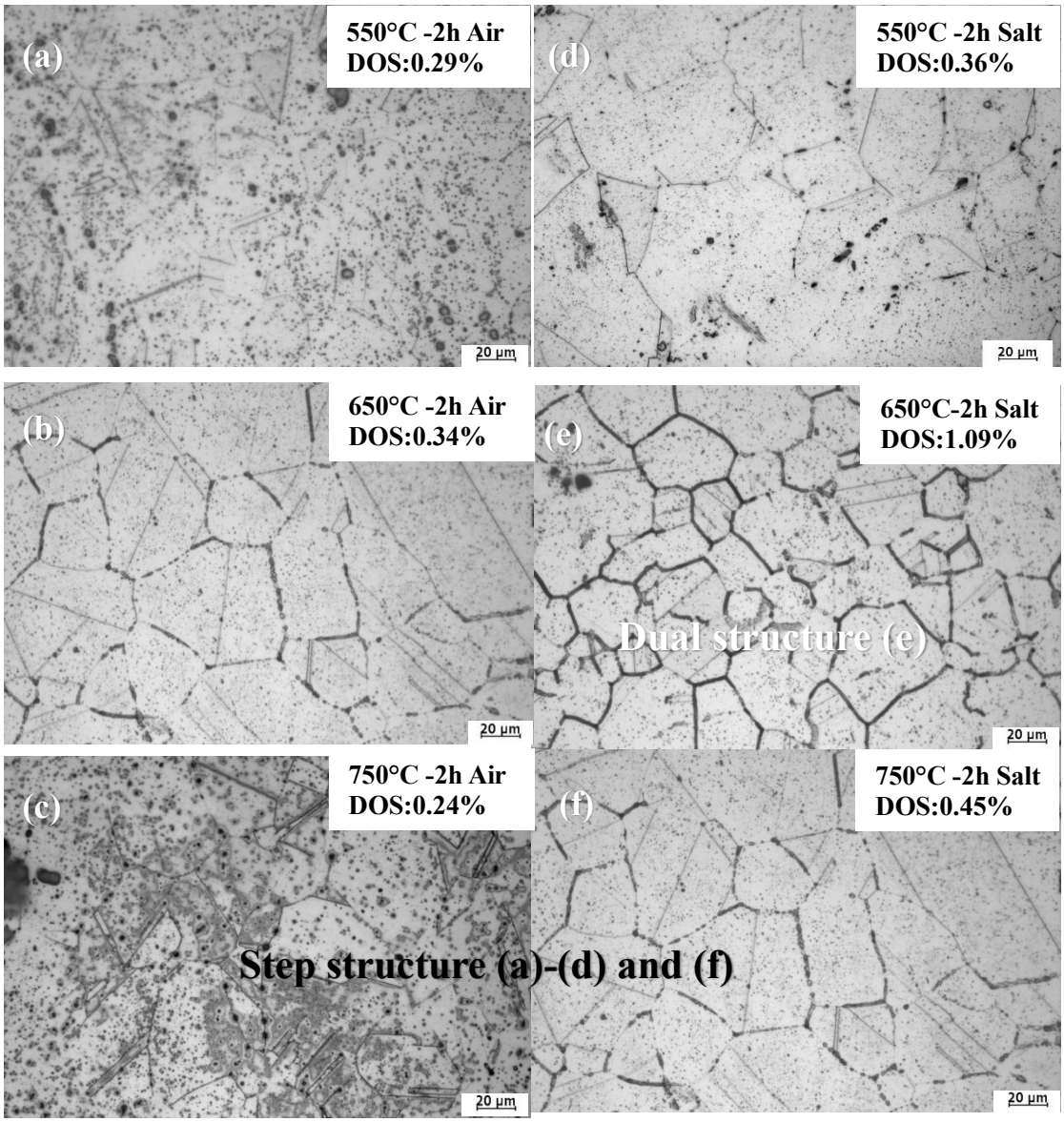

Figure 12 Oxalic etching microstructures for AISI 347 treated by (a) 550°C for 2 h in air; (b) 650°C for 2 h in air; (c) 750°C for 2 h in air; (d) 550°C for 2 h in molten salt; (e) 650°C for 2 h in molten salt; (f) 750°C for 2 h in molten salt, respectively.

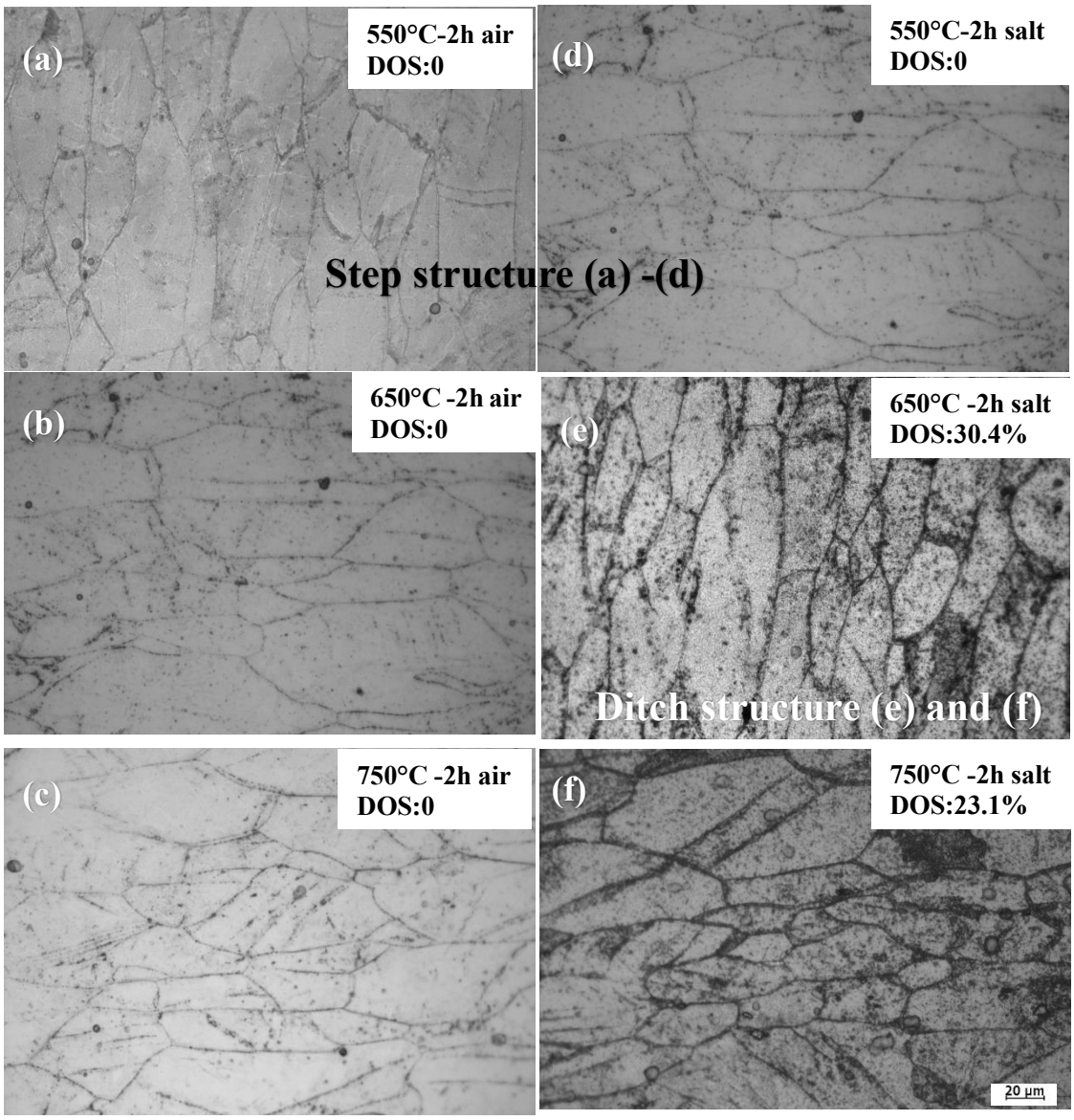

Figure 13 Oxalic etching microstructures for IN 625 treated by (a) 550°C for 2h in air; (b) 650°C for 2h in air; (c) 750°C for 2h in air; (d) 550°C for 2h in molten salt; (e) 650°C for 2h in molten salt; (f) 750°C for 2h in molten salt ,respectively.

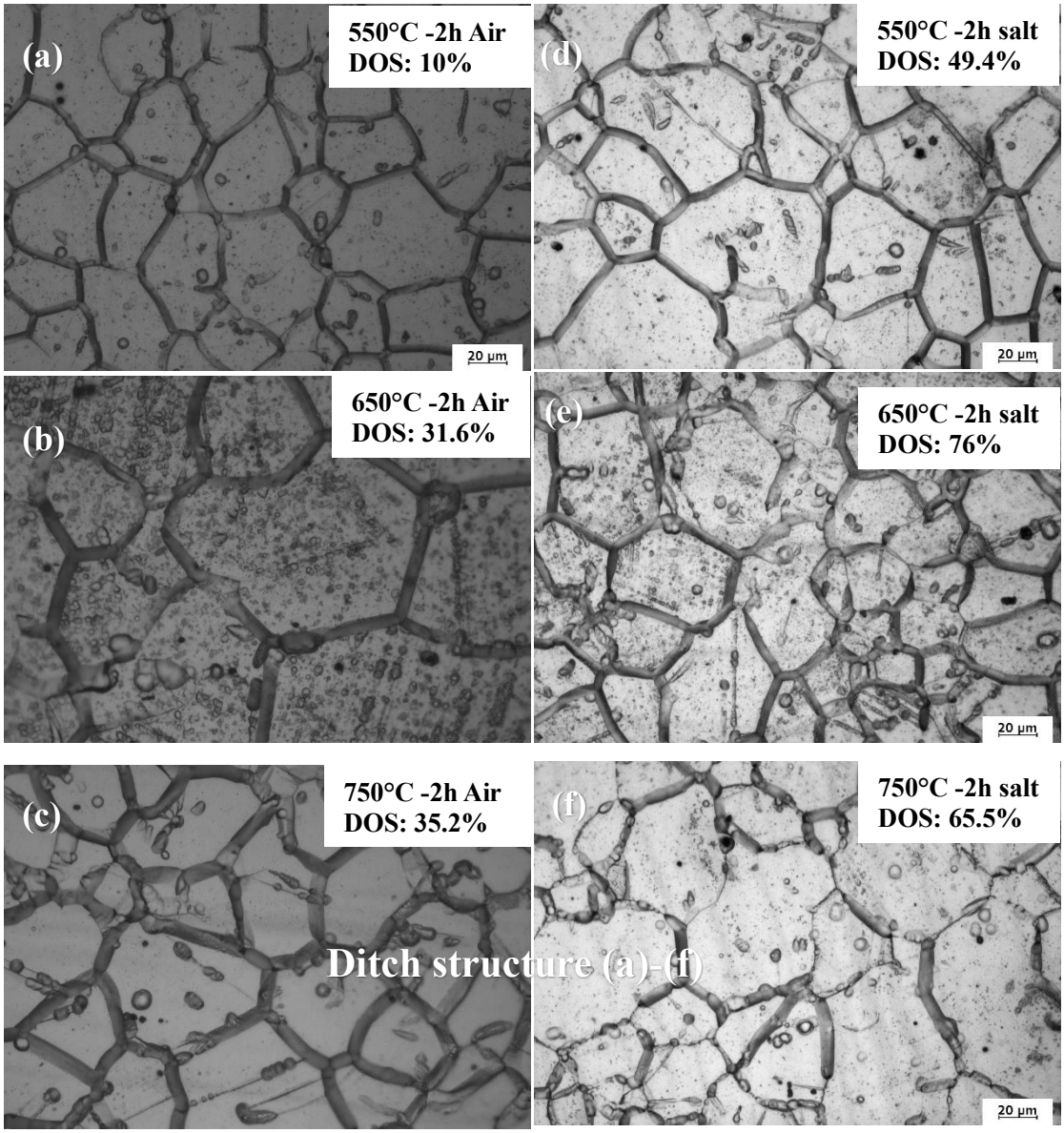

Figure 14 Oxalic etching microstructures for In 825 treated by (a) 550°C for 2 h in air; (b) 650°C for 2 h in air; (c) 750°C for 2 h in air; (d) 550°C for 2 h in molten salt; (e) 650°C for 2 h in molten salt; (f) 750°C for 2 h in molten salt, respectively.

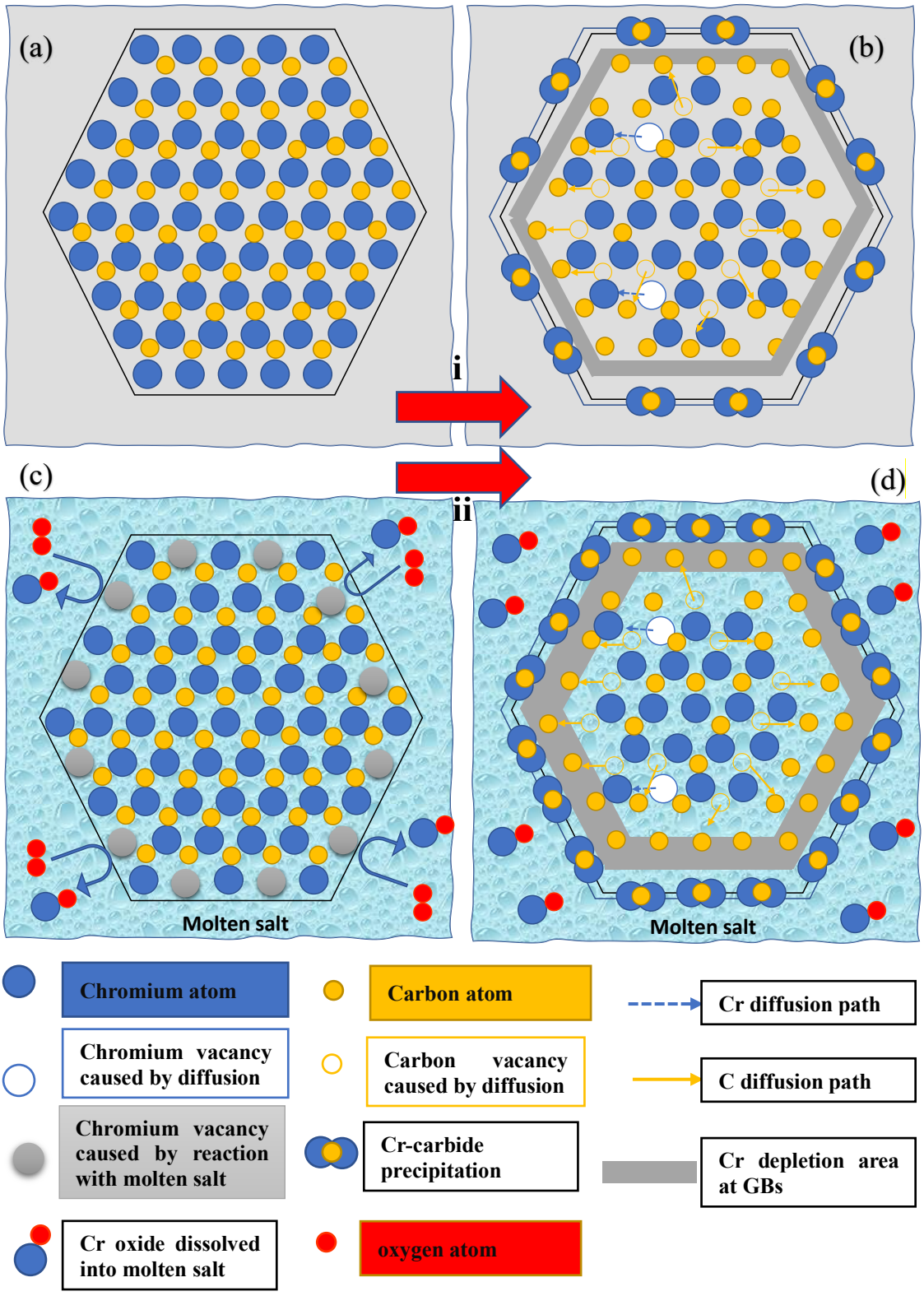

Figure 15 Schematic of sensitization mechanism on the surface of stainless steels/Ni-based alloys (a) and (b) in air, (c) and (d) in molten salts.

6. References

[1] M. Walczak, F. Pineda, Á.G. Fernández, C. Mata-Torres, R.A. Escobar, Materials corrosion for thermal energy storage systems in concentrated solar power plants, Renewable and Sustainable Energy

Reviews 86 (2018) 22-44.
[2] U. Pelay, L. Luo, Y. Fan, D. Stitou, M. Rood, Thermal energy storage systems for concentrated solar power plants, Renewable and Sustainable Energy Reviews 79 (2017) 82-100.
[3] G. Alva, Y. Lin, G. Fang, An overview of thermal energy storage systems, Energy 144 (2018) 341-378.
[4] U. Desideri, P.E. Campana, Analysis and comparison between a concentrating solar and a photovoltaic power plant, Applied Energy 113 (2014) 422-433.
[5] A.S. Lima, A.M. Nascimento, H.F.G. Abreu, P. de Lima-Neto, Sensitization evaluation of the austenitic stainless steel AISI 304L, 316L, 321 and 347, Journal of Materials Science 40(1) (2005) 139-144.
[6] E.A. Trillo, L.E. Murr, Effects of carbon content, deformation, and interfacial energetics on carbide precipitation and corrosion sensitization in 304 stainless steel, Acta Materialia 47(1) (1998) 235-245.
[7] F.G. Wilson, Mechanism of Intergranular Corrosion of Austenitic Stainless Steels—Literature Review, British Corrosion Journal 6(3) (1971) 100-108.
[8] Y. Yin, R.G. Faulkner, P. Moreton, I. Armson, P. Coyle, Grain boundary chromium depletion in austenitic alloys, Journal of Materials Science 45(21) (2010) 5872-5882.
[9] H. Sahlaoui, H. Sidhom, J. Philibert, Prediction of chromium depleted-zone evolution during aging of Ni–Cr–Fe alloys, Acta Materialia 50(6) (2002) 1383-1392.
[10] J. Qian, C. Chen, H. Yu, F. Liu, H. Yang, Z. Zhang, The influence and the mechanism of the precipitate/austenite interfacial C-enrichment on the intergranular corrosion sensitivity in 310S stainless steel, Corrosion Science 111 (2016) 352-361.
[11] P. Gellings, M.J.C.s. De Jongh, Grain boundary oxidation and the chromium-depletion theory of intercrystalline corrosion of austenitic stainless steels, 7(7) (1967) 413-421.
[12] S. Kolli, V. Javaheri, T. Ohligschläger, J. Kömi, D. Porter, The importance of steel chemistry and thermal history on the sensitization behavior in austenitic stainless steels: Experimental and modeling assessment, Materials Today Communications 24 (2020) 101088.
[13] P. Lejček, Models of equilibrium grain boundary segregation, Grain Boundary Segregation in Metals, Springer2010, pp. 51-102.
[14] A. Pardo, M.C. Merino, A.E. Coy, F. Viejo, M. Carboneras, R. Arrabal, Influence of Ti, C and N concentration on the intergranular corrosion behaviour of AISI 316Ti and 321 stainless steels, Acta Materialia 55(7) (2007) 2239-2251.
[15] H.-J. Kim, S.-H. Jeon, S.-T. Kim, I.-S. Lee, Y.-S. Park, K.-T. Kim, Y.-S. Kim, Investigation of the sensitization and intergranular corrosion of tube-to-tubesheet welds of hyper duplex stainless steel using an electrochemical reactivation method, Corrosion Science 87 (2014) 60-70.
[16] H. Kokawa, M. Shimada, Y.S. Sato, Grain-boundary structure and precipitation in sensitized austenitic stainless steel, JOM 52(7) (2000) 34-37.
[17] S.-X. Li, Y.-N. He, S.-R. Yu, P.-Y. Zhang, Evaluation of the effect of grain size on chromium carbide precipitation and intergranular corrosion of 316L stainless steel, Corrosion Science 66 (2013) 211-216.
[18] T. Thorvaldsson, G.L. Dunlop, Effect of stabilizing additions on precipitation reactions in austenitic stainless steel, Metal Science 16(4) (1982) 184-190.
[19] T. Thorvaldsson, G.L. Dunlop, Precipitation reactions in Ti-stabilized austenitic stainless steel, Metal Science 14(11) (1980) 513-518.
[20] T. Thorwaldsson, G. Dunlop, The influence of composition on precipitation in stabilized austenitic stainless steels, Strength of Metals and Alloys 1 (1979) 755-760.

[21] A.S. Grot, J.E. Spruiell, Microstructural stability of titanium-modified type 316 and type 321 stainless steel, Metallurgical transactions A 6(11) (1975) 2023-2030.
[22] F. Perrard, A. Deschamps, F. Bley, P. Donnadieu, P. Maugis, A small-angle neutron scattering study of fine-scale NbC precipitation kinetics in the [alpha]-Fe-Nb-C system, Journal of Applied Crystallography 39(4) (2006) 473-482.
[23] F. Perrard, A. Deschamps, P. Maugis, Modelling the precipitation of NbC on dislocations in α-Fe, Acta Materialia 55(4) (2007) 1255-1266.
[24] D. West, J. Hulance, R.L. Higginson, G.D. Wilcox, σ-phase precipitation in 347HFG stainless steel, Materials Science and Technology 29(7) (2013) 835-842.
[25] X. Zhang, J. Tang, H. Liu, J. Gong, Effects of pre-strain on sensitization and interganular corrosion for 304 stainless steel, Engineering Failure Analysis 106 (2019) 104179.
[26] M. Hofmeister, L. Klein, H. Miran, R. Rettig, S. Virtanen, R.F. Singer, Corrosion behaviour of stainless steels and a single crystal superalloy in a ternary LiCl–KCl–CsCl molten salt, Corrosion Science 90 (2015) 46-53.
[27] B. Grégoire, C. Oskay, T.M. Meißner, M.C. Galetz, Corrosion mechanisms of ferritic-martensitic P91 steel and Inconel 600 nickel-based alloy in molten chlorides. Part I: NaCl–KCl binary system, Solar Energy Materials and Solar Cells 215 (2020) 110659.
[28] S.H. Goods, R.W. Bradshaw, M.R. Prairie, J.M. Chavez, Corrosion of stainless and carbon steels in molten mixtures of industrial nitrates, Office of Scientific and Technical Information (OSTI), 1994.
[29] S. Bell, T. Steinberg, G. Will, Corrosion mechanisms in molten salt thermal energy storage for concentrating solar power, Renewable and Sustainable Energy Reviews 114 (2019).
[30] E. Hamdy, J.N. Olovsjö, C. Geers, Perspectives on selected alloys in contact with eutectic melts for thermal storage: Nitrates, carbonates and chlorides, Solar Energy 224 (2021) 1210-1221.
[31] K. Morshed-Behbahani, P. Najafisayar, M. Pakshir, M. Shahsavari, An electrochemical study on the effect of stabilization and sensitization heat treatments on the intergranular corrosion behaviour of AISI 321H austenitic stainless steel, Corrosion Science 138 (2018) 28-41.
[32] A. Bonk, M. Braun, V.A. Sötz, T. Bauer, Solar Salt – Pushing an old material for energy storage to a new limit, Applied Energy 262 (2020) 114535.
[33] M. Mehos, C. Turchi, J. Vidal, M. Wagner, Z. Ma, C. Ho, W. Kolb, C. Andraka, A. Kruizenga, Concentrating solar power Gen3 demonstration roadmap, National Renewable Energy Lab.(NREL), Golden, CO (United States), 2017.
[34] BS EN ISO 12732:2008 Corrosion of metals and alloys. Electrochemical potentiokinetic reactivation measurement using the double loop method (based on Cihal's method), BSI, 2008.
[35] A. International, ASTM A262-15, Standard Practices for Detecting Susceptibility to Intergranular Attack in Austenitic Stainless Steels, PA, West Conshohocken, 2015.
[36] A. Mahmoudi, M. Esmailian, S. Aghamiri, Effect of Stabilizing Heat Treatment on Intergranular Corrosion Resistance of Welded Stainless Steel AISI 321, Advanced Materials Research 535-537 (2012) 692-696.
[37] A. Gomes, M. Navas, N. Uranga, T. Paiva, I. Figueira, T.C. Diamantino, High-temperature corrosion performance of austenitic stainless steels type AISI 316L and AISI 321H, in molten Solar Salt, Solar Energy 177 (2019) 408-419.
[38] R.W. Bradshaw, S.H. Goods, Corrosion of alloys and metals by molten nitrates, Sandia National Lab.(SNL-CA), Livermore, CA (United States), 2001.
[39] M.A. Stopher, P. Lang, E. Kozeschnik, P.E.J. Rivera-Diaz-Del-Castillo, Modelling hydrogen

migration and trapping in steels, Materials & Design 106 (2016) 205-215.
[40] T. Sourmail, Precipitation in creep resistant austenitic stainless steels, Materials science and technology 17(1) (2001) 1-14.
[41] T. Kekkonen, P. Aaltonen, H. Hanninen, Intergranular corrosion testing of nickel-base alloys, Scand. J. Metall. 14(5) (1985) 243-251.
[42] V.r. Číhal, R. Štefec, On the development of the electrochemical potentiokinetic method, Electrochimica Acta 46(24) (2001) 3867-3877.
[43] G.S. Was, H.H. Tischner, R.M. Latanision, INFLUENCE OF THERMAL TREATMENT ON THE CHEMISTRY AND STRUCTURE OF GRAIN BOUNDARIES IN INCONEL 600, Metallurgical transactions. A, Physical metallurgy and materials science 12 A(8) (1981) 1397-1408.
[44] A. Soleimani Dorcheh, R.N. Durham, M.C. Galetz, Corrosion behavior of stainless and low-chromium steels and IN625 in molten nitrate salts at 600 °C, Solar Energy Materials and Solar Cells 144 (2016) 109-116.
[45] M. Sarvghad, T.A. Steinberg, G. Will, Corrosion of steel alloys in eutectic NaCl+Na2CO3 at 700°C and Li2CO3 + K2CO3 + Na2CO3 at 450°C for thermal energy storage, Solar Energy Materials and Solar Cells 170 (2017) 48-59.
[46] O. Ahmed, Corrosion behaviour of AISI 304 stainless steel in contact with eutectic salt for concentrated solar power plant applications, (2013).